Title
Prediction of Rotorcraft Broadband Trailing-Edge Noise and Parameter Sensitivity Study

Journal
Proceedings of the Vertical Flight Society 75th Annual Forum and Technology Display

Authors
Li, Sicheng
Lee, Seongkyu

Publication Date
2019-05-13

DOI
10.4050/f-0075-2019-14442

Prediction of Rotorcraft Broadband Trailing-Edge Noise and Parameter Sensitivity Study

Sicheng Li
Ph.D. Student

Seongkyu Lee
Assistant Professor

Department of Mechanical and Aerospace Engineering
University of California, Davis
Davis, California, 95616 U.S.A.

ABSTRACT

This paper investigates effects of rotorcraft design and operating parameters on its trailing-edge noise. A rotor trailing-edge noise prediction method is first developed, where the aerodynamics and the turbulence wall pressure spectrum near the trailing edge on airfoils are predicted by a combination of the standard blade element momentum theory (BEMT), a viscous boundary-layer panel method, and a recently developed empirical wall pressure spectrum model. The coordinate transformations are combined with the Amiet model to predict far-field noise. Compared to experimental data, the validation of this method demonstrates its advantage and validity for airfoil and rotorcraft broadband noise predictions. Thereafter, this method is used to study effects of rotorcraft design and operating parameters on rotor trailing-edge noise. It is found that the tip Mach number is a dominant factor for rotor trailing-edge noise. It is found that the broadband noise scales with the 5.5^{th} power of the rotor tip Mach number. Detailed trend analyses of noise levels as a function of frequency are presented in terms of collective pitch angle, twist angle, blade chord length, and rotor radius. It is found that the collective pitch angle, twist angle, and the chord length make noticeable impacts on the low- and mid-frequency noise. A dipole noise directivity is observed, and the directivity and geometric attenuation of rotor trailing-edge noise can be well represented by a semi-analytic equation.

NOTATION

c	chord length, m
c_o	speed of sound, m/s
C_f	skin friction coefficient
C_T	thrust coefficient
D	rotor diameter, m
D_ϕ	directivity term
dp/dx	pressure gradient, Pa/m
E^*	complex conjugate of a Fresnel integral
f	frequency, Hz
k_x	chordwise wavenumber
L	effective lift function
l_r	spanwise turbulence lengthscale, m
M	freestream Mach number
M_r	rotational Mach number
M_{β_p}	flapping motion matrix
M_t	rotor tilt motion matrix
M_{tip}	tip Mach number
M_θ	blade twist and collective pitch matrix
M_ϕ	azimuth motion matrix
N	number of sections on a blade
N_B	number of blade
OASPL	overall sound pressure level, dB
PWL	sound power level, dB
R	rotor radius
R_o	observer-hub distance, m
R_s	observer-blade section distance, m
r	radial position of a blade section midspan, m
$\mathrm{SPL}_{i(U/L)}$	blade section (upper or lower surface) sound pressure level, dB
$\mathrm{SPL}_{\mathrm{rotor}}$	rotor sound pressure level, dB
S_{pp}	azimuthally averaged acoustic PSD
$\bar{S}_{pp}$	instantaneous acoustic PSD
t	rotor tilt, deg
U_c	convective velocity, m/s
U_e	boundary layer edge velocity, m/s
U_∞	freestream velocity, m/s
u_τ	friction velocity, $(\tau_w/\rho)^{1/2}$
V_c	ascending speed, m/s
X,Y,Z	source local coordinate system
X_1,Y_1,Z_1	observer global coordinate system
β_p	blade flap, deg
β_1,β_2,β_3	constant scaling parameters
Δr	blade section span
δ	boundary layer thickness, m
δ^*	boundary layer displacement thickness, m
Θ	momentum thickness, m
θ	blade twist, deg

Presented at the Vertical Flight Society 75th Annual Forum & Technology Display, Philadelphia, Pennsylvania, May 13–16, 2019.

θ_0	collective pitch, deg
ν	kinematic viscosity, m^2/s
ρ	fluid density, kg/m^3
τ_w	wall shear stress, Pa
Φ_{pp}	surface pressure spectrum, $\mathrm{Pa}^2 \cdot \mathrm{s}$
ϕ	blade azimuth angle, deg
Ψ	elevation angle, deg
Ω	rotor rotational speed, rad/s
ω	source frequency, rad/s
ω_d	Doppler-shifted frequency, rad/s

INTRODUCTION

Noise from rotorcraft can be categorized into tonal noise and broadband noise by its nature. While rotorcraft tonal noise is typically dominant at low and mid frequencies, broadband noise covers a wide frequency range including high frequency, at which human ears are sensitive. Historically, less research effort has been devoted to rotorcraft broadband noise compared to its tonal noise. However, rotorcraft broadband noise becomes important when the tonal noise is weak. Recently, interest in broadband noise has been raised with the broader use of rotorcraft and the emergence of urban air mobility vehicle concepts. To demonstrate the importance of rotor broadband noise on traditional helicopters, Snider et al. (Ref. 1) measured helicopter fly-over noise and found that rotor broadband noise is important at over-head position, which contribute significantly to Effective Perceived Noise Level (EPNL). For small-scale rotors, Intaratep et al. (Ref. 2) experimentally showed that broadband noise of DJI Phantom rotor, especially trailing-edge noise, not only dominates at the mid and high-frequency ranges, but also considerably increases from a single rotor to multi-rotors. In addition, the acoustic measurements by Zawodny et al. (Ref. 3) showed that quadcopter rotors generate considerable broadband noise above 1kHz frequency and the A-weighted spectrum (Ref. 4) indicates human ear's high sensitivity in such frequency range.

Trailing-edge noise is a type of broadband noise that contributes significantly to mid and high-frequency noise. This noise is generated by the interaction between a turbulent boundary layer flow and a trailing-edge corner on an airfoil section or a flat plate. Trailing-edge noise models on an airfoil have been empirically and theoretically developed. A semi-empirical BPM model was developed by Brooks et al. (Ref. 9) and has been widely used to predict airfoil self-noise. Theoretically, Ffowcs Williams et al. (Ref. 7) provided a trailing-edge noise solution to the Lighthill (Ref. 8) acoustic analogy equation. Likewise, using the theory of Curle (Ref. 5), Amiet (Ref. 6) developed a theoretical model to predict trailing-edge noise on an airfoil.

Schlinker et al. (Ref. 10) applied the Amiet airfoil trailing-edge noise model to predict helicopter trailing-edge noise, but their prediction had some critical limitations. Firstly, an airfoil was modeled as a flat plate, which could not well represent actual boundary layer flow properties. Secondly, the blade section freestream velocity was described by the combination of rotational and axial velocity, which neglected the induced velocities on the rotor plane. Thirdly, blade noise was assumed to be generated at the rotor hub location, which resulted in errors in the actual source-observer distance. Kim and George (Ref. 11) predicted trailing-edge noise from a hovering rotor from the rotating source formulation of Ffowcs Williams and Hawkings (Ref. 12) with the power spectral density given in the Amiet model. In their method, however, each blade was modeled as a point source of a flat plate, and the effect of an angle of attack was neglected. More recently, Blandeau et al. (Ref. 13) improved the first limitation of Schlinker et al. by replacing the flat plate by an airfoil and predicted propeller trailing-edge noise, but the wall pressure spectrum was obtained from Goody's model (Ref. 14), which was developed for zero pressure gradient flows on a flat plate and is not accurate for airfoil adverse pressure gradient flows. In addition, they assumed that the observer and propeller were in the same vertical plane and neglected the effects of skewed gust. They also considered the noise source as a point source that is located at 75% of the blade radius. As for the method of accounting for the blade sections as the noise sources, Brooks and Burley (Ref. 15) used coordinate transformations to locate the blade sections at the noise source locations by including the rotor tilt angle, the sectional radius, and the blade azimuthal angle for the prediction of blade wake interaction noise. However, their transformations did not include the blade twist angle, the flapping angle, and the collective and cyclic pitching angles.

In this paper, an improved prediction method named UCD-QuietFly is developed to predict rotor trailing-edge noise. This method utilizes multiple coordinate transformations during the motions of rotor blades to account for each blade section as a noise source and individually compute each blade section's noise contribution to a given observer. The blade twist angle, collective pitch angle, flapping angle, azimuthal angle, sectional radius, and rotor tilt angle are included in the coordinate transformation. The new model combines Blade Element Momentum Theory (BEMT), the XFOIL boundary-layer panel code, and a recently developed empirical wall pressure spectrum model (Ref. 16) to accurately obtain the source of trailing-edge noise at given flight conditions of rotorcraft. Following its development, UCD-QuietFly is validated against airfoil trailing-edge noise and rotor noise measurements in hover.

For an airfoil section, the effects of flow Mach number, angle of attack, and chord length on the trailing-edge noise were studies by other researches. Hutcheson and Brooks (Ref. 19) computationally and experimentally showed that the airfoil trailing edge noise is well scaled with the fifth power of the flow Mach number and that the angle of attack only affects low-frequency noise. For the same effective angle of attack, Brooks and Pope (Ref. 9) experimentally showed, with a boundary-layer tripped airfoil, that the larger chord length increased the noise level and shifted the level peak to a lower frequency. Lee (Ref. 25) also studied the effect of the airfoil shape on trailing-edge noise using a TNO-Blake model. He identified the noise source region and showed that the suction side contributes to the low-frequency noise and the pressure side contributes to the high-frequency noise. On a rotorcraft, Chou and George (Ref. 20) found that collective pitch angle has a large effect on the low-frequency and the mid-frequency noise while it has a negligible effect on the high-frequency noise.

In the second part of this paper, UCD-QuietFly is used to study the effects of rotor tip Mach number, collective pitch, blade twist, chord length, rotor radius, and ascending speed on rotor trailing-edge noise. Finally, the rotor noise directivity is analyzed, and a semi-analytic equation is proposed to represent the geometric attenuation and the directivity of rotorcraft trailing-edge noise.

METHOD

In this section, the formulations of UCD-QuietFly are presented. We use Amiet's power spectral density (PSD) $\overline{S}_{pp}$ (Ref. 6) at an observer location (X,Y,Z) of each surface of an airfoil as

$$\overline{S}_{pp} = \frac{1}{32\pi^2}\left(\frac{\omega_d c Z}{c_o \sigma^2}\right)^2 \Delta r |L|^2 l_r \Phi_{pp}, \tag{1}$$

where $\sigma^2 = X^2 + \beta^2\left(Y^2+Z^2\right)$, $\beta^2 = 1 - M^2$, ω_d is the Doppler-shifted frequency, c is the chord length, c_o is the speed of sound, Δr is the blade sectional span, Z has the coordinate in Fig. 1, L is the loading term, l_r is the spanwise turbulence correction length, and Φ_{pp} is the wall pressure spectrum. The blade sectional local coordinate is shown in Fig. 1; for each section on a blade, the origin of the local coordinate is located at the mid-span of the section.

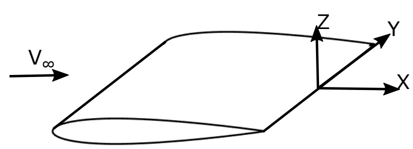

Fig. 1: Blade section local coordinate.

The motion of rotor blades is included in the coordinate transformation. The twist angle matrix M_θ, the azimuth motion matrix M_ϕ, the tilt motion matrix M_t, and flapping motion matrix M_{β_p} transform the geographical global coordinate (X_1,Y_1,Y_1) shown in Fig. 2 to the sectional local coordinate (X,Y,Z) shown in Fig. 1.

$$\begin{bmatrix} X \\ Y \\ Z \end{bmatrix} = M_\theta M_\phi \left[M_t \begin{bmatrix} X_1 \\ Y_1 \\ Z_1 \end{bmatrix} + M_{\beta_p} \right] \tag{2}$$

where M_θ, M_ϕ, M_t, and M_{β_p} are defined as

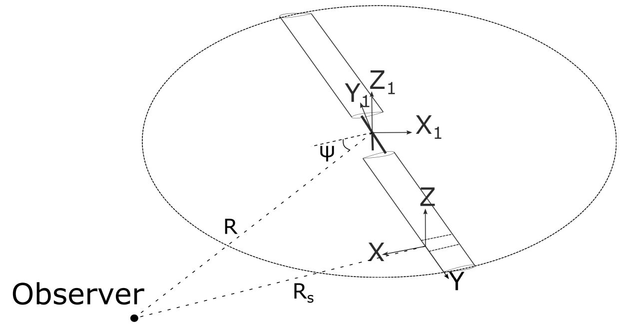

Fig. 2: Airfoil local and global coordinates for an observer.

$$\begin{aligned}
M_\theta &= \begin{bmatrix} \cos(\theta_0+\theta) & 0 & \sin(\theta_0+\theta) \\ 0 & 1 & 0 \\ -\sin(\theta_0+\theta) & 0 & \cos(\theta_0+\theta) \end{bmatrix}, \\
M_\phi &= \begin{bmatrix} \sin\phi & -\cos\phi & 0 \\ \cos\phi & \sin\phi & 0 \\ 0 & 0 & 1 \end{bmatrix}, \\
M_t &= \begin{bmatrix} \cos t & 0 & \sin t \\ 0 & 1 & 0 \\ -\sin t & 0 & \cos t \end{bmatrix}, \\
M_{\beta_p} &= \begin{bmatrix} -r\sin\beta_p\cos\phi \\ -r\sin\beta_p\sin\phi \\ r\cos\beta_p \end{bmatrix}.
\end{aligned} \tag{3}$$

where θ_0 describes the collective pitch angle that varies with the rotor thrust, θ describes the twist angle and the cyclic pitch angle, ϕ describes the azimuth angle, t describes the tilt angle with positive angle tilting up, r describes the blade sectional distance from the hub, and β_p describes the flapping angle. To authors' best knowledge, none of the earlier research included the entire blade motions, with the flapping, collective pitch, cyclic pitch, and twist angles, in the prediction of rotor trailing-edge noise. Even though cyclic flapping and pitch angles are not present in hover, they should be included in forward flight.

The PSD of each section changes with the azimuth angle, hence it is azimuthally averaged by

$$S_{pp} = \frac{N_B}{2\pi}\int_0^{2\pi}\left(\frac{\omega}{\omega_d}\right)^2 \overline{S}_{pp} d\phi, \tag{4}$$

in which the Doppler-shifted frequency ω_d at the observer is related to the source frequency ω using

$$\frac{\omega_d}{\omega} = \frac{1}{1+M_r\left(\dfrac{X}{R_s}\right)}. \tag{5}$$

Note that $M_r = \Omega r/c_o$ is the rotational Mach number of the blade section. X has the direction pointing from leading edge to trailing edge shown in Fig. 2, and R_s is the distance between the blade section and an observer. Substituting Eq. (1) and

Eq. (5) into Eq. (4) and expanding the terms give the acoustic PSD generated from each blade section as

$$S_{pp} = \left(\frac{\omega}{c_o}\right)^2 c^2 \triangle r \left(\frac{1}{32\pi^2}\right) \frac{B}{2\pi} \int_0^{2\pi} D_\phi |L|^2 l_r \Phi_{pp} d\phi, \quad (6)$$

where the directivity term is given as $D_\phi = \left(Z/\sigma^2\right)^2$, and the local coordinate of Z and σ must be found by taking the coordinate transformations in Eqs. (2) - (3) from the global coordinate. A detailed equation of the directivity term D_ϕ in terms of the global coordinate system (X_1, Y_1, Z_1) are provided in the Appendix.

The loading term L is given by Amiet (Ref. 10) as

$$\begin{aligned}|L| = \frac{1}{\Lambda}|e^{i2\Lambda}[1-(1+i)E^*\left(2\left(\overline{K}+\overline{\mu}M+\overline{\gamma}\right)\right) \\ + e^{-i2\Lambda}\sqrt{\frac{K+\mu M+\gamma}{\mu x/\sigma+\gamma}}(1+i)E^*\left(2\left(\overline{\mu}x/\sigma+\overline{\gamma}\right)\right)]|\end{aligned} \quad (7)$$

where $\Lambda = \overline{k}_x - \overline{\mu}x/\sigma + \overline{\mu}M$, $K = \omega_d/U_c$, $\mu = \omega_d M/U\beta^2$, $\gamma^2 = (\mu/\sigma)^2(x^2+\beta^2 z^2)$, and E^* represents the complex conjugate of a Fresnel integral. The turbulence convective velocity and the spanwise turbulence length scale are defined as $U_c = 0.8U_\infty$ and $l_r = 1.6U_c/\omega$, respectively, where the constants 0.8 and 1.6 will be used for rotorcraft noise predictions.

The remaining wall pressure spetrum Φ_{pp} is obtained by a recently developed empirical wall pressure spectrum model for non-zero gradient flows, the Lee's model (Ref. 16), as

$$\frac{\Phi_{pp}(\omega)U_e}{\tau_w^2\delta^*} = \frac{max(a,(0.25\beta_c-0.52)a)(\frac{\omega\delta^*}{U_e})^2}{[4.76(\frac{\omega\delta^*}{U_e})^{0.75}+d^*]^e+[8.8R_T^{-0.57})(\frac{\omega\delta^*}{U_e})]^{h^*}} \quad (8)$$

where $\beta_c = (\Theta/\tau_w)(dp/dx)$, $a = 2.28\Delta^2(6.13\Delta^{-0.75}+d)^e[4.2(\Pi/\Delta)+1]$, $\Delta = \delta/\delta^*$, $\Pi = 0.8(\beta_c+0.5)^{3/4}$, $e = 3.7+1.5\beta_c$, $d = 4.76(1.4/\Delta)^{0.75}[0.375e-1]$, $R_T = (\delta/U_e)(\nu/u_\tau^2)$, $h^* = \min(3,(0.139+3.1043\beta_c))+7$, and if $(\beta_c < 0.5)$, $d^* = \max(1.0, 1.5d)$, otherwise $d^* = d$.

Finally, the far-field SPL for one side of the i^{th} section is calculated from the power spectral density S_{pp} as

$$\mathrm{SPL}_{i(U/L)} = 10\log_{10}\left(\frac{2\pi S_{pp}}{(2\times10^{-5})^2}\right), \quad (9)$$

where U and L represent the upper and lower surfaces of an airfoil, respectively. The rotor's total SPL is logarithmically summed to be

$$\mathrm{SPL}_{\mathrm{rotor}} = 10\log_{10}\sum_{i=1}^{N}\left(10^{0.1\mathrm{SPL}_{iU}}+10^{0.1\mathrm{SPL}_{iL}}\right), \quad (10)$$

where N is the total number of sections.

During the prediction process, the blade sectional freestream velocity and the angle of attack are obtained from Blade Element Momentum Theory (BEMT) in hover, and the boundary-layer flow parameters, which are inputs to Eq. (8), are obtained from XFOIL (Ref. 24).

RESULTS

The predictions of trailing-edge noise from UCD-QuietFly are first validated against measurement data for airfoil and helicopter noise. After the validation, this prediction tool is used to perform a trend analysis of trailing-edge noise associated with rotor design and operating parameters, such as the rotor tip Mach number, ascending speed, radius, blade collective pitch angle, twist angle, and chord length. The detailed flow physics behind this noise trend is also discussed. A semi-analytic equation is obtained from a noise map on the plane observers.

A. Validation

This section first shows the validation of airfoil trailing-edge noise predictions to demonstrate the accuracy of the numerical method on one blade section. Next, two experimental cases of hovering helicopters are used to demonstrate the validity of UCD-QuietFly. In addition, the UCD-QuietFly predictions are compared with the predictions by Kim and George (Ref. 11). For the validations against the two rotorcraft cases, 40 sections are used on each blade, and 240 airfoil panels are used in the XFOIL. The computational time to obtain the noise level is 65 seconds.

1. Airfoil Trailing-Edge Noise Validation: Airfoil trailing-edge noise is predicted and compared with the measurement, which was reported in Benchmark Problems for Airframe Noise Computations (BANC) (Ref. 17). Table 1 describes the airfoil test conditions. For this airfoil validation case, the turbulence convective velocity $U_c = 0.7U_\infty$ and spanwise turbulence lengthscale $l_r = 1.0U_c/\omega$ are used (Ref. 18).

Table 1: Airfoil Test Conditions.

Item	Value
Airfoil	NACA0012
Chord Length[m]	0.4
Span[m]	1.0
(X,Y,Z)[m]	(0.0, 0.0, 1.0)
Fixed Transition Position (x/c)	S[1]: 0.06, P:0.07
U_∞[m/s]	53.0
Angle of Attack[deg]	6

[1]S: Suction Side, P: Pressure Side

One-third octave band sound pressure levels (SPLs) of airfoil trailing-edge noise prediction and the measurement are presented in Fig. 3, in which error bars of ±3dB are included. The prediction has a good match with the measurement, which demonstrates the validity of the numerical approach involving the boundary-layer flow parameters from

XFOIL, the Lee's wall pressure spectrum model in Eq. (8), and the Amiet model in Eq. (1).

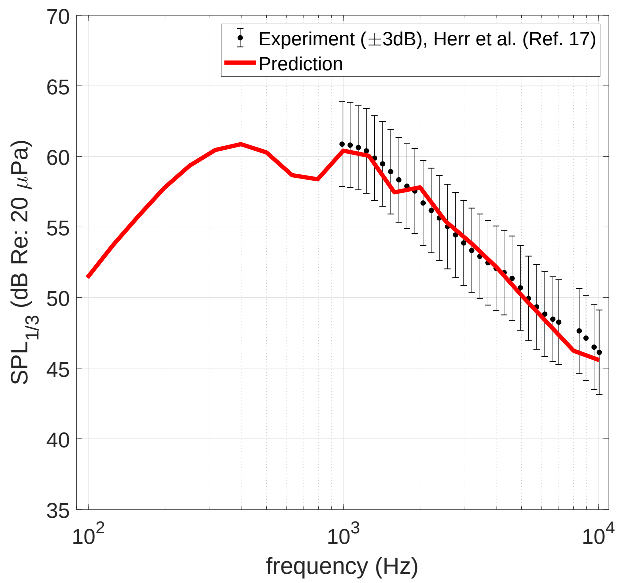

Fig. 3: Airfoil trailing-edge noise prediction against measuremnt (Ref. 17).

2. Rotor Tailing-Edge Noise Validation Case 1: In Table 2, the helicopter configuration in the experiment conducted by Johnson et al. (Ref. 22) is shown, where the observer is 5 rotor diameters from the hub with an elevation angle of $\Psi = 26.7°$. In the experiment, a UH-1B helicopter was used.

Table 2: Configuration of Case 1.

Case	Johnson (Ref. 22)
Radius[m]	6.7056
Airfoil	NACA0012
Number of Blade	2
Linear Twist[deg]	-10
Solidity	0.0506
(X_1, Y_1, Z_1)[m]	(60.69, 0, -30.48)
(R_o, Ψ)[m, deg]	(67.91, -26.7)
C_T	0.0036
M_{tip}	0.67

The prediction of Johnson case is presented in Fig. 4 along with the measurement and the prediction by Kim and George (Ref. 11). The result shows that UCD-QuietFly has a good match with the measurement in the mid- and high-frequency range, in which trailing-edge noise is expected to be the dominant noise source. In addition, Fig. 4 shows that UCD-QuietFly is more accurate than Kim and George's prediction for the entire frequency range.

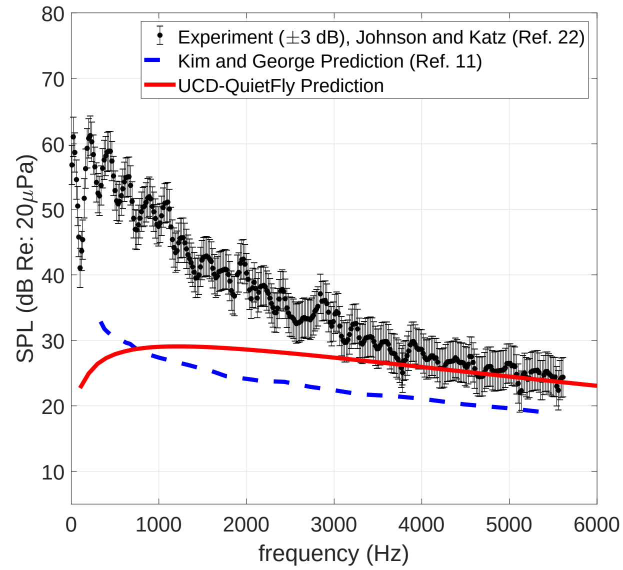

Fig. 4: Prediction against measurement by Johnson (Ref. 22), and prediction by Kim and George (Ref. 11).

3. Rotor Tailing-Edge Noise Validation Case 2: In Table 3, Leverton (Ref. 23) measured noise from a model rotor at an observer located at 4.5 rotor diameters from the hub with an elevation angle of $\Psi = 75°$.

Table 3: Configuration of Case 2.

Case	Leverton (Ref. 23)
Radius[m]	8.5
Airfoil	NACA0012
Number of Blade	2
Linear Twist[deg]	-8
Solidity	0.0312
(X_1, Y_1, Z_1)[m]	(19.7, 0, -73.6)
(R_o, Ψ)[m, deg]	(76.19, 75)
C_T	0.002
M_{tip}	0.47

The prediction of the Leverton case is presented in Fig. 5. Note that the SPL in Fig. 5 has a constant frequency bandwidth of 100 Hz and sums the 1-Hz energy in each band. In particular, the prediction exhibits similar trends with the data. In particular, the prediction is in good agreement with the data at high frequencies. The prediction does not capture the local noise maximum at 2.5-4 kHz. It is thought that this local noise maximum is generated from different noise sources such as trailing-edge bluntness noise.

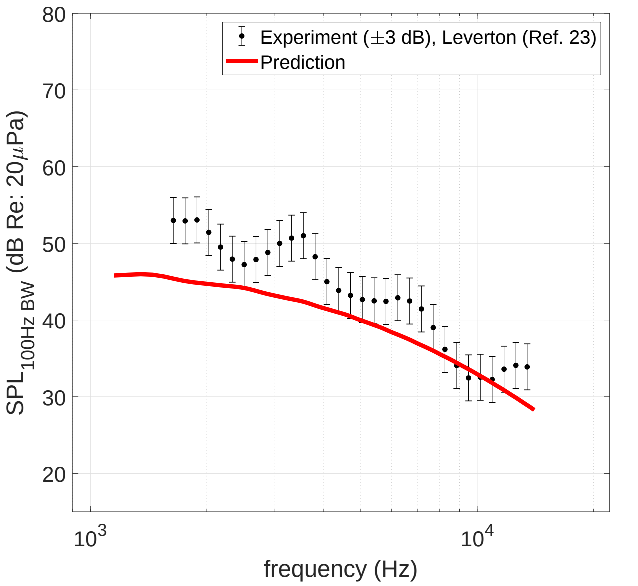

Fig. 5: Prediction against measurement by Leverton (Ref. 23).

B. Rotor Parameters Trend Analysis

In this subsection, UCD-QuietFly is used to investigate the trend of rotor trailing-edge noise with different parameters. Six parameters studied are listed in Table 4, and other constant conditions are shown in Table 5. Each parameter is analyzed from the start to the end values while other parameters are kept at the base values. For each parameter, 20 values were selected. An observer is located at one base rotor diameter from the hub with $-90°$ degree elevation angles.

Table 4: Range of Parameters.

Parameter	Start	End	Base
M_{tip}	0.45	0.8	0.67
θ_0[deg]	11	18	13.52
θ[deg]	-13	-4	-10
Chord Length [m]	0.4	0.75	0.53
Rotor Radius [m]	2.3	8.0	6.7056
V_c [m/s]	0	9	0

Table 5: Constant Conditions.

Item	Value
Airfoil	NACA0012
(R_o, Ψ)[m, deg]	(13.4112, -90)
N_B	2

The trends of the overall sound pressure level (OASPL) associated with the rotorcraft design and operating parameters are presented in Fig. 6. It is seen that the OASPL increases with the increased tip Mach number, collective pitch angle, blade twist angle, chord length, and rotor radius, but the ascending speed has a small effect on the rotor trailing-edge noise. The blade pitch angle, twist angle, chord length changes OASPL only by about 2 dB within the specified ranges. The rotor radius changes OASPL by about 5 dB. Among the studied parameters, the tip Mach number is found to be the dominant factor on the rotorcraft trailing-edge noise. Although Fig. 6 indicates the general effects of the parameters, detailed studies of the parameters are provided in the following sections to show the narrow-band sound pressure levels and the flow physics in terms of the boundary layer parameters.

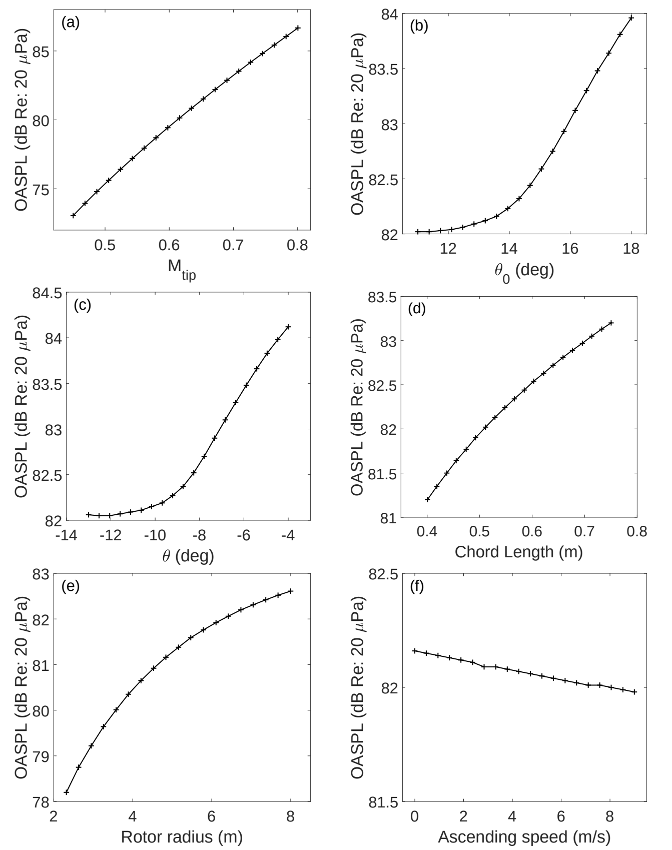

Fig. 6: OASPL trend with parameters: (a) tip Mach number, (b) collective pitch angle, (c) blade linear twist slope, (d) blade chord length, (e) rotor radius, (f) rotor ascending speed.

1. Effect of rotor tip Mach number: The trend of narrow-band sound pressure level associated with the rotor tip Mach number is shown in Fig. 7. It is shown that the narrow-band SPL increases with increasing the tip Mach number for the entire frequency range. This trend is explained by the boundary layer parameters at 90% rotor radius position as shown in Fig. 8. The noise increase is mainly accounted for the increase in the boundary layer edge velocity U_e and the pressure gradient dp/dx near the trailing edge. The higher tip Mach number gives a higher boundary layer edge velocity and a higher convection velocity. According to Eq. (8), the strength of the wall pressure spectrum is proportional to the boundary layer edge velocity, and the higher wall pressure spectrum results in a higher noise level. In addition to the increase in the magnitude of SPL, the increased tip Mach number shifts the spectral peak to a higher frequency.

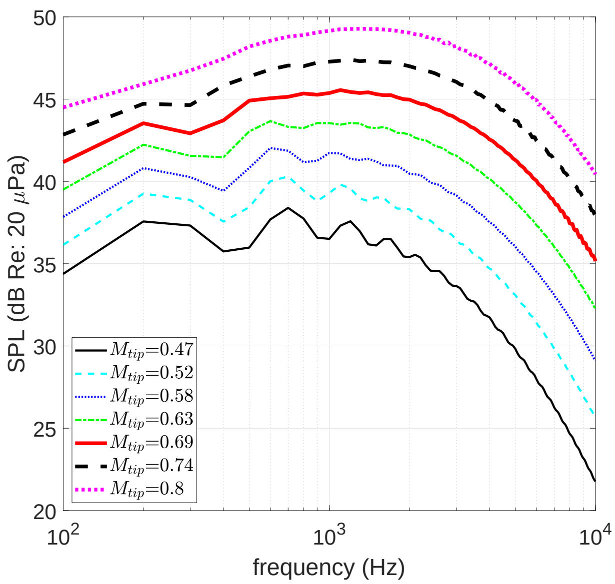

Fig. 7: Noise trend associated with tip Mach number.

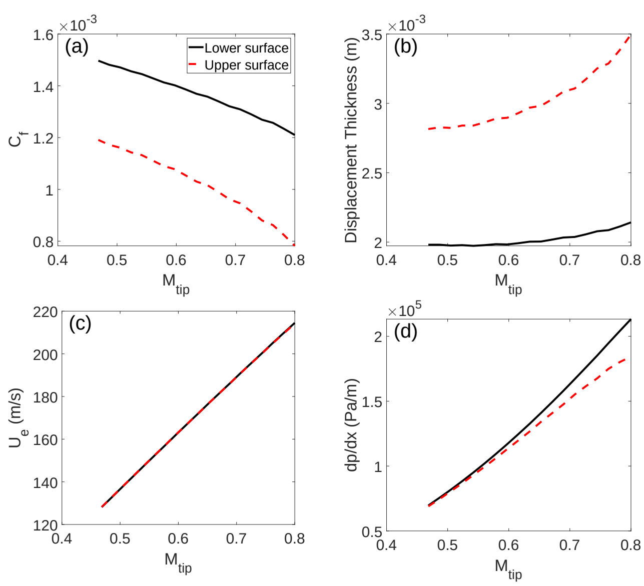

Fig. 8: Tip Mach number: boundary layer parameters at 90% rotor radius.

In Fig. 9, the sound pressure level is scaled with the 5.5^{th} power of the tip Mach number, and the frequency is normalized with the tip Mach number to collapse the maximum peak frequency. It is found that SPLs collapse very well into a single line, especially for high Mach number cases, with the 5^{th} power of the tip Mach number and the frequency scaling of $f * 0.8/M_{tip}$. The rotor tip Mach number scaling between two rotors is provided in Eq. (11), which is close to the flow Mach number's 5^{th} power scaling on an airfoil as suggested by Hutcheson and Brooks (Ref. 19).

$$\mathrm{SPL}_{\mathrm{rotor},1} = \mathrm{SPL}_{\mathrm{rotor},2} + 10\log_{10}\left[\left(\frac{M_{tip,1}}{M_{tip,2}}\right)^{5.5}\right] \tag{11}$$

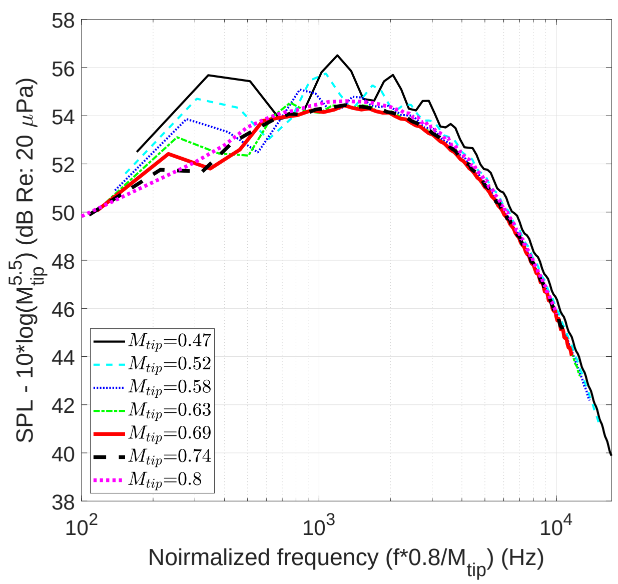

Fig. 9: Scaled SPL with tip Mach number.

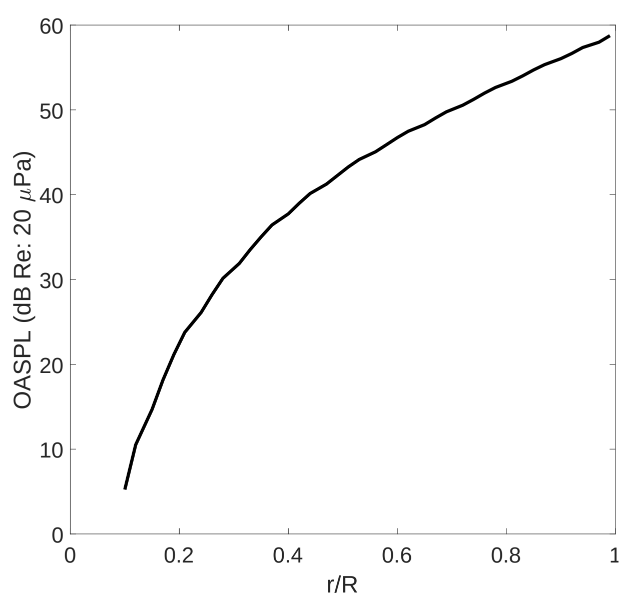

Fig. 10: Sectional noise contribution from one blade.

With a constant rotor radius, the overall sound pressure level contribution from each blade section is plotted in Fig. 10. Since the tip sections have a higher velocity than the root section, the trailing-edge noise level from the tip sections are higher.

2. Effect of blade collective pitch: Collective pitch angle changes the angle of attack on the entire blade. Figure 11 shows that increasing collective pitch angle gives higher low-frequency noise while high-frequency (larger than 5kHz) noise remains unchanged. In Fig. 12 (b), as the angle of attack increases, the boundary-layer displacement thickness increases on the upper surface and decreases on the lower surface. It is also found that the change in the edge velocity U_e is very small and the pressure gradients decrease with increasing the collective pitch angle. The upper and lower surfaces contribute to the low and high frequency noise. Although Hutcheson and Brooks (Ref. 19) showed that the angle of attack only affects noise with frequencies lower than 1kHz, Fig. 11 demonstrates the collective pitch angle's influence on frequency lower than 5kHz for rotorcraft noise.

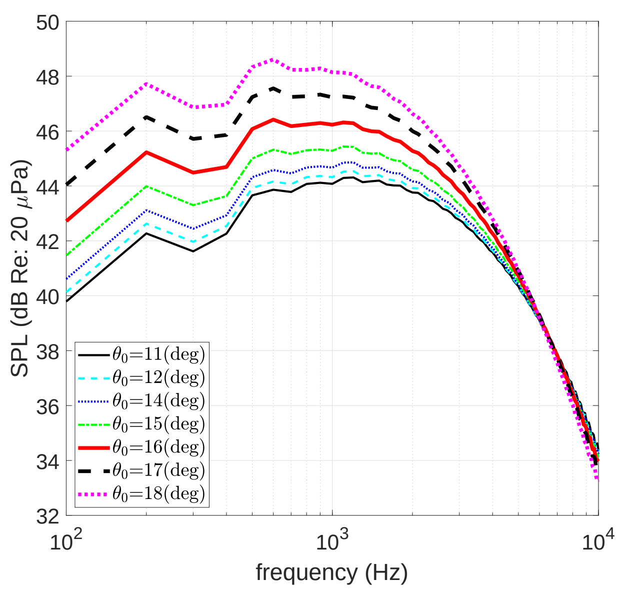

Fig. 11: Noise trend associated with colletive pitch angle.

Chou and George's results (Ref. 20) based on Kim and George method (Ref. 11) showed that the effect of the collective pitch on the low-frequency (100 Hz) and the mid-frequency (1000 Hz) noise were the same. However, Fig. 11 shows that the effect at the low-frequency is larger than that at the mid-frequency.

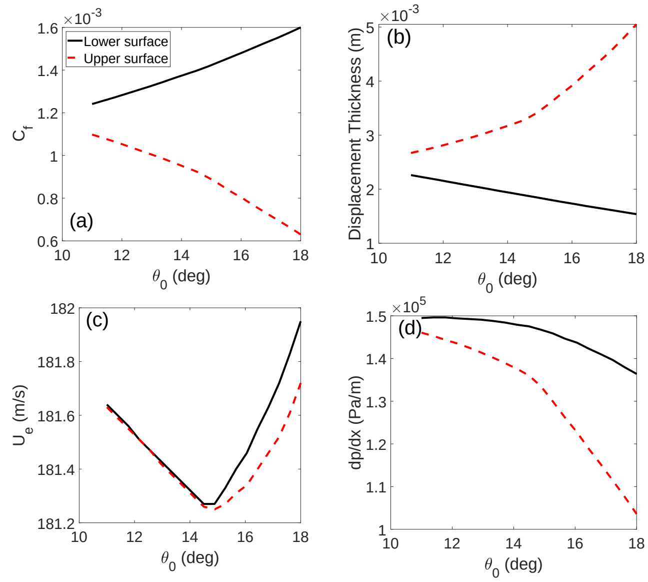

Fig. 12: Collective pitch angle: boundary layer parameters at 90% rotor radius.

3. Effect of blade twist: Unlike the collective pitch angle, blade twist angle increases with the blade radius. Figure 13 shows the SPL as a function of the linear twist slope from the root to the tip. The noise trend with the twist angle, is similar to the trend of collective pitch. In fact, the behaviors of the boundary-layer parameters, shown in Fig. 13, are very similar to those for the collective pitch angle.

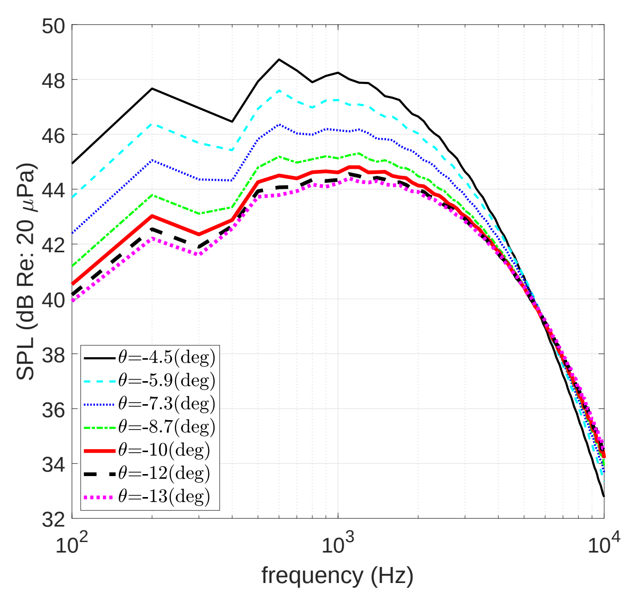

Fig. 13: Noise trend associated with the linear blade twist slope.

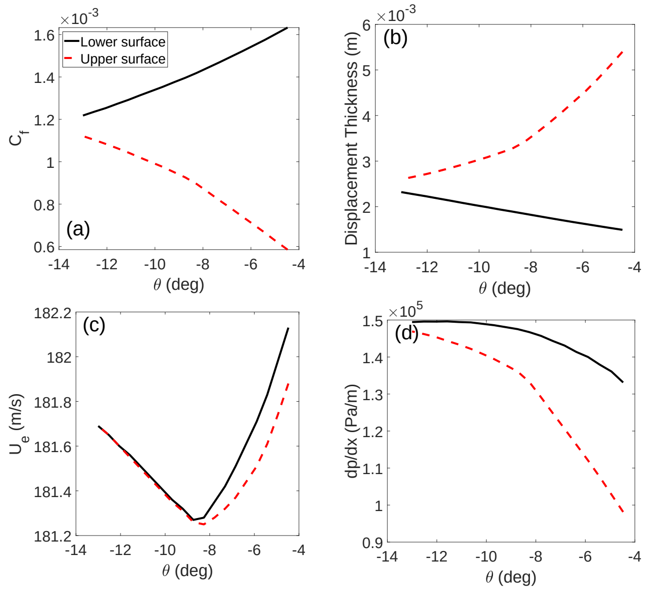

Fig. 14: Blade twist: boundary layer parameters at 90% rotor radius.

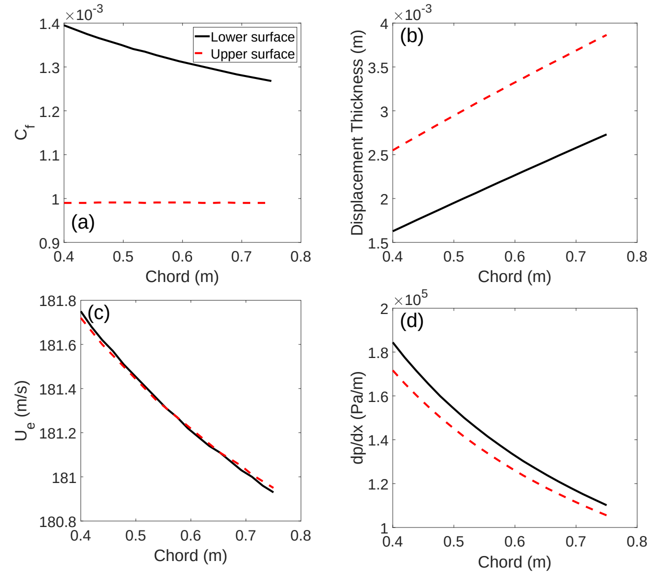

Fig. 16: Chord length: boundary layer parameters at 90% rotor radius.

4. Effect of blade chord length: Figure 15 shows the SPLs as a function of the blade chord length. The increase in chord length results in higher low-frequency noise while the high-frequency noise remains unchanged. Since the boundary layer develops further with longer a chord length, the boundary layer becomes thicker, especially on the upper surface, as shown in Fig. 16 (b), which accounts for the increase in low-frequency noise. In addition, the peak level shifts to lower frequencies as the chord length is increased, which agrees with the effect of a chord length on an airfoil noise (Ref. 9).

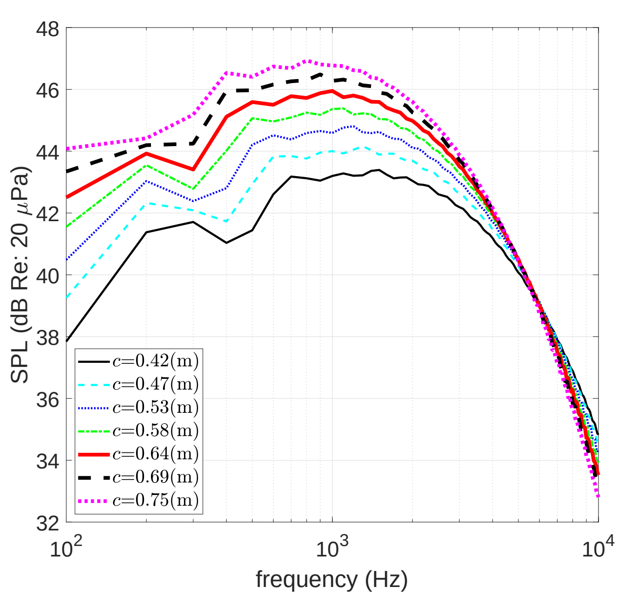

Fig. 15: Noise trend associated with blade chord length.

5. Effect of rotor radius: Figure 18 shows the SPLs as a function of the blade radius with the same tip Mach number. It is shown that the increased rotor radius gives higher sound pressure levels in the entire frequency range. The boundary-layer parameter changes at 90% rotor radius are small as shown in Fig. 17 because the tip Mach number is kept constant. The main factor accounting for the noise increase is the span increase with increasing the rotor radius. In other words, the source region is increased with increasing the blade radius.

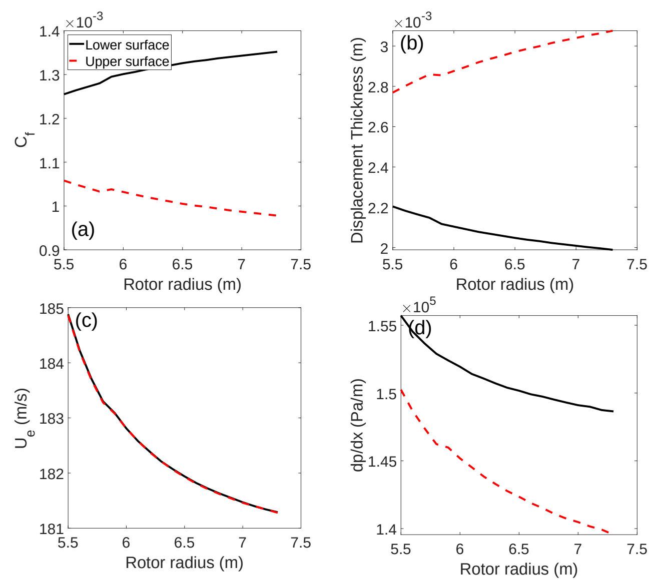

Fig. 17: Rotor radius: boundary layer parameters at 90% rotor radius.

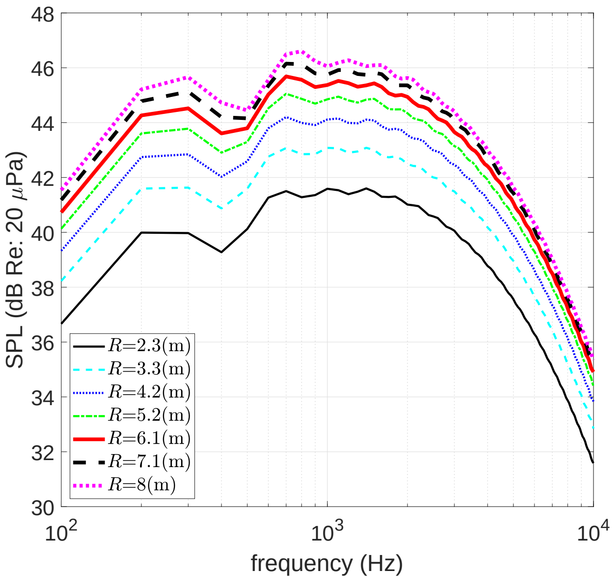

Fig. 18: Noise trend associated with rotor radius.

6. Effect of rotor ascending speed: Figure 19 shows the SPLs as a function of the rotor climb or ascending speed. An increased ascending speed slightly increases the noise level. The effect is small compared to the other rotor parameters because the variation of the local angle of attack is small within the limited realistic ascending speed range, which is 9 m/s for this rotor. Figure 20 shows that the changes in the boundary-layer parameters are small with the ascending speed.

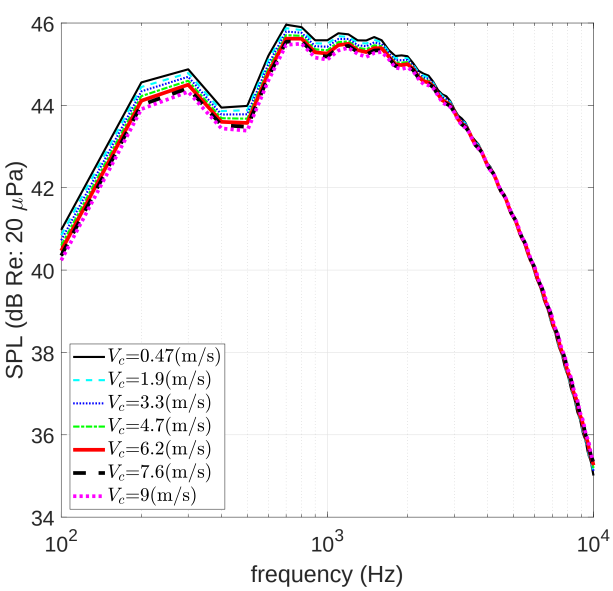

Fig. 19: Noise trend associated with rotor ascending speed.

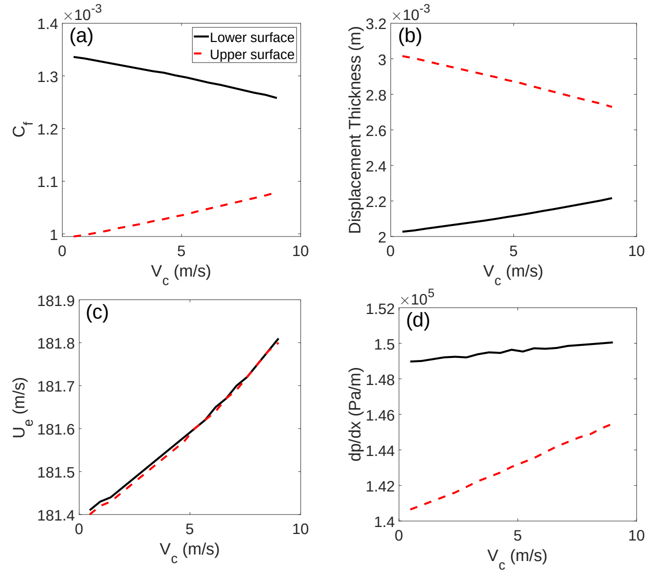

Fig. 20: Ascending speed: boundary layer parameters at 90% rotor radius.

C. Rotor Geometric Attenuation and Directivity

The geometric attenuation and directivity pattern of rotor trailing-edge noise are studied, and a semi-analytic equation is obtained to relate the overall sound pressure level at any observer locations to that at a reference location of one rotor diameter with $-90°$ elevation angle. Using the base values in Table 4, the overall sound pressure level is predicted by UCD-QuietFly on the X_1Y_1 and X_1Z_1 planes shown in Fig. 21-22. Table 6 provides the detailed coordinate ranges about these two planes. The dipole directivity is shown in Fig. 21 when the noise levels are viewed from the side of rotorcraft. When the noise levels are viewed from the top in Fig. 22, the noise contours have a monopole directivity.

Table 6: Geometric Attenuation and Directivity.

	X_1Y_1	X_1Z_1
X_1 Range[m]	[-70,70]	[-30,30]
Y_1 Range[m]	[-70,70]	NA
Z_1 Range[m]	NA	[-100,-10]
Grid Size[m]	10	5
Distance to Hub[m]	-26.8	0

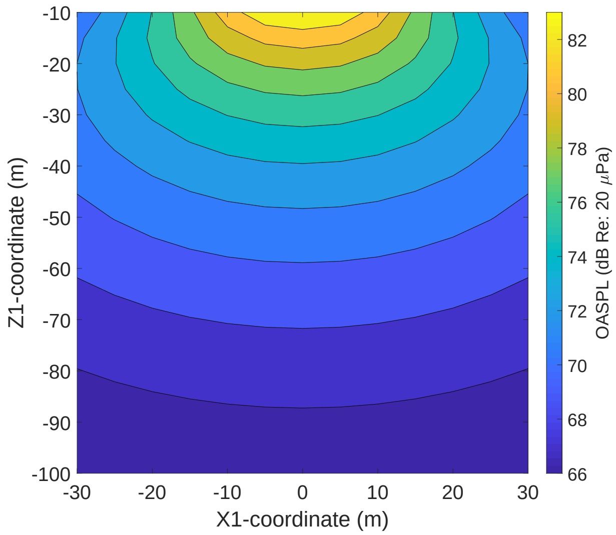

Fig. 21: OASPL on X_1Z_1 plane from UCD-QuietFly.

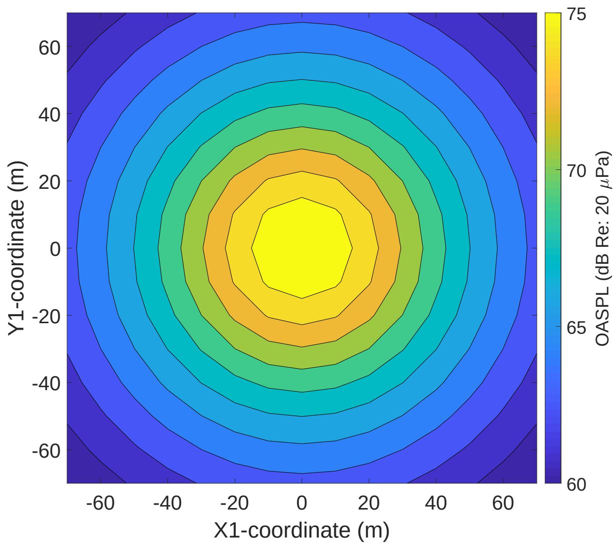

Fig. 22: OASPL on X_1Y_1 plane from UCD-QuietFly.

The ISO standard (Ref. 21) gives the geometric attenuation of a point source as shown in Eq. (12), where PWL_{ref} is sound power level at a point source.

$$\text{SPL} = \text{PWL}_{\text{ref}} - [20\log(R) + 11] \tag{12}$$

However, Eq. (12) cannot be directly applied to predict rotorcraft noise at far field since the noise source is not a point source. In addition, rotor trailing-edge noise has a dipole directivity, which should be included in far-field noise predictions. The rotor geometric attenuation equation is proposed to have a form of Eq. (13), in which the first term accounts for the directivity at one rotor diameter distance while the second term couples the effect of the attenuation and directivity. The constants β_1, β_2, and β_3 are determined by minimizing the difference between this equation and the noise predicted on the X_1Y_1 and X_1Z_1 planes. $\text{OASPL}_{\text{ref}}$ is the overall sound pressure level at one rotor diameter with $-90°$ elevation angle.

$$\text{OASPL} = (\sin^{\beta_1}|\phi|)\text{OASPL}_{\text{ref}} - [\beta_2 + \beta_3(1 - \sin|\phi|)]\log\left(\frac{R}{d}\right) \tag{13}$$

Based on the prediction results as shown in Fig. 21-22, the Quasi-Newton minimization method is used to find the three constants as

$$\beta_1 = 0.0209; \qquad \beta_2 = 18.2429; \qquad \beta_3 = 6.7267 \tag{14}$$

Figure 23 shows the the overall sound pressure level calculated by Eq (13), where its average difference in comparison with the direct UCD-QuietFly predictions is 0.0147 dB, or 0.018% of the OASPL. Such a small difference demonstrates a good representation of the combination of rotor noise attenuation and directivity in the proposed semi-analytic equation form. The difference between the UCD-QuietFly and Eq (13) are presented in Fig. 23 (c)-(d), demonstrating the close match except for small elevation angles.

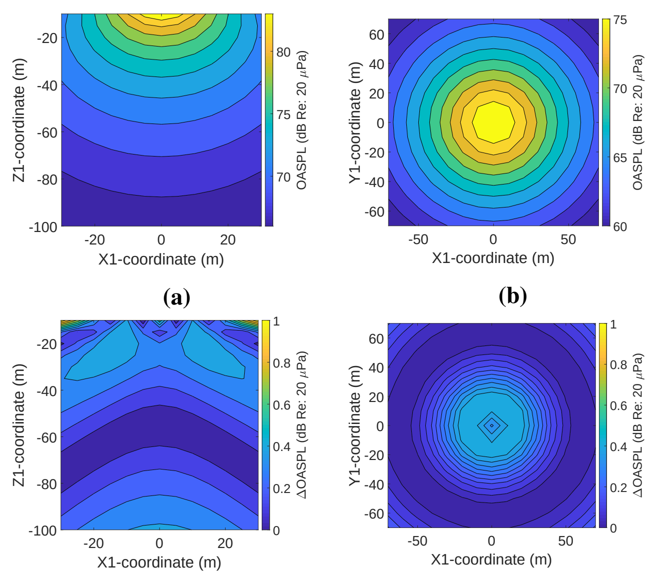

Fig. 23: OASPL calculated from rotor attenuation equation, and its difference to UCD-QuietFly. (a) OASPL calculated by Eq. (13) on the X_1Z_1 plane, (b) OASPL calculated by Eq. (13) on the X_1Y_1 plane, (c) Absolute difference between Fig. 23 (a) and Fig. 21 on the X_1Z_1 plane, (d) Absolute difference between Fig. 23 (b) and Fig. 22 on the X_1Y_1 plane.

SPL predicted by Eq. (13) is compared with UCD-QuietFly results of multiple elevation angles and distances in Fig. 24. It is shown that Eq. (13) predicts an accurate attenuation and the directivity, except for small elevation angle. Figure 24 also shows that at low elevation angles, the noise reduction is steeper with increasing the observer distance. It is worthwhile noting that it is possible to predict noise levels at the entire observer plane with only one noise level at a reference position and Eq. (13). Considering the computation time of about 1 min at a single observer using UCD-QuietyFly and instant calculations of Eq. (13), the computational time saving using this approach is a factor of N, where N denotes the number of observers.

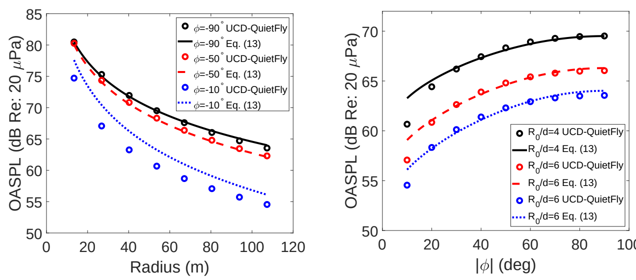

(a) **(b)**

Fig. 24: Comparison of UCD-QuietFly and Eq. (13).

CONCLUSION

This paper presented a new computational approach to predict rotor trailing-edge noise in blade full motion. The method combined the BEMT, XFOIL, an empirical wall pressure spectrum model, and Amiet model to predict the local angle of attack, boundary-layer parameters, turbulence wall pressure spectrum, and trailing-edge noise. The numerical code, which is referred to as UCD-QuietFly, was validated against measurement data for airfoil noise and helicopter noise in hover. Key foundings are summarized as follows:

1. Rotor trailing-edge noise is scaled with the 5.5^{th} power of the tip Mach number and the frequency is scaled with $f*0.8/M_{tip}$.

2. Although the effect the of rotational speed still dominates the rotor trailing-edge noise, neglecting other parameters results in considerable inaccuracies. For example, an increased collective pitch angle increased the noise levels at low- to mid-frequencies while maintaining the high-frequency noise. The blade twist angle was observed to have a similar effect as the collective pitch angle. An increased chord length only increases the low- to mid-frequency noise levels. An increased rotor radius with the constant tip Mach number results in higher noise for all frequencies mainly due to the increased source region. Finally, an increased ascending speed shows the limited effect on rotor trailing-edge noise due to the operational limit of the helicopter maximum ascending speed.

3. For a hovering helicopter, the vertical plane (X_1Y_1) has a dipole shape directivity pattern while the horizontal plane (X_1Y_1) has a circular monopole directivity pattern. A semi-analytic equation was proposed to represent the geometric attenuation and directivity of rotor trailing-edge noise. This equation requires SPL at one reference observer location, which can be obtained by UCD-Quietfly or any other methods including measurement. It was shown that this proposed equation provided good agreement with direct noise computations on the observer plane except shallow elevation angles. The computational time saving of an order of the number of observers can be achieved using this semi-analytic equation.

APPENDIX

The expanded form of the directivity term D_ϕ is shown in Eq. (a-1), which is obtained by performing the coordinate transformations in Eq. (2)-(3).

$$\begin{aligned} D_\phi = A_1 \cdot ((\sin(\theta_0+\theta)(r\cos\beta_p + Z_1\cos t - X_1 \sin t) \\ + \cos(\theta_0+\theta)\sin\phi \cdot A_2 - \cos(\theta_0+\theta)\cos\phi \cdot A_3)^2 \\ + A_1 + (\cos\phi * A_2 + \sin\phi \cdot A_3)^2)^{-2} \end{aligned} \tag{a-1}$$

A_1, A_2, and A_3 in Eq. (a-1) are shown as follows for clarity.

$$\begin{aligned} A_1 = (\cos(\theta_0+\theta)(r\cos\beta_p + Z_1\cos t - X_1\sin t) \\ - \sin(\theta_0+\theta)\sin\phi \cdot A_2 + \sin(\theta_0+\theta)\cos\phi \cdot A_3)^2 \end{aligned} \tag{a-2}$$

$$A_2 = X_1\cos t + Z_1 \sin t - r\cos\phi \sin\beta_p \tag{a-3}$$

$$A_3 = Y_1 - r\sin(\beta_p)\sin(\phi) \tag{a-4}$$

REFERENCES

[1]Snider, R., Samuels, T., Goldman, B., and Brentner, K., "Full-Scale Rotorcraft Broadband Noise Prediction and Its Relevance to Civil Noise Certification Criteria," 69th AHS Annual Forum, Phoenix, AZ, May 21-23, 2013.

[2]Intaratep, N., Alexander, W, and Devenport, W., "Experimental Study of Quadcopter Acoustics and Performance at Static Thrust Conditions," 22nd AIAA/CEAS Aeroacoustics Conference, Lyon, France, May 30-June 1, 2016.

[3]Zawodny, N., Boyd, D., and Burley, C., "Acoustic characterization and prediction of representative, small-scale rotary-wing unmanned aircraft system components," 72nd AHS Annual Forum, West Palm Beach, FL, May 17-19, 2016.

[4]Zawodny, N., and Boyd, D., "Investigation of rotor-airframe interaction noise associated with small-scale rotary-wing unmanned aircraft systems," 73rd AHS Annual Forum, Fort Worth, TX, May 9-11, 2017.

[5]Curle, N., “The Influence of Solid Boundaries upon Aerodynamic Sound,” *Proceedings of the Royal Society*, A231, 1955, pp. 505-514.

[6]Amiet, R., “Acoustic Radiation from an Airfoil in a Turbulent Stream,” *Journal of Sound and Vibration*, Vol. 41, (4), 1975, pp. 407-420.

[7]Ffowcs Williams, J.E., and Hall, L., “Aerodynamic Sound Generation by Turbulent Flow in the Vicinity of a Scattering Half Plane,” *Journal of Fluid Mechanics*, Vol. 40, (4), 1970, pp. 657-670.

[8]Lighthill, M., “On Sound Generated Aerodynamically I. General Theory,” *Proceedings of the Royal Society*, A211, 1952, pp. 564-587.

[9]Brooks, T.F., Pope, D.S., and Marcolini, M.A., “Airfoil Self-noise and Prediction,” NASA RP 1218, 1989.

[10]Schlinker, R.H., and Amiet, R.K., “Helicopter Rotor Trailing Edge Noise,” NASA RP 3470, 1981.

[11]Kim, Y.N., and George, A.R, “Trailing-Edge Noise from Hovering Rotors,” *AIAA Journal*, Vol. 20, (9), 1982, pp. 1167-1174.

[12]Ffowcs Williams, J.E., and Hawkings, D.L., “Theory Relating to the Noise of Rotating Machinery,” *Journal of Fluid Mechanics*, Vol. 10, (1), 1969, pp. 10-21.

[13]Blandeau, V., and Joseph, P., “Validity of Amiet’s Model for Propeller Trailing-Edge Noise,” *AIAA Journal*, Vol. 49, (5), 2011, pp. 1057-1066.

[14]Goody, M., “Empirical Spectral Model of Surface Pressure Fluctuations,” *AIAA Journal*, Vol. 42, (9), 204, pp. 1788-1794.

[15]Brooks, T.F., and Burley, C.L., “Blade Wake Interaction Noise for a Main Rotor,” *Journal of the American Helicopter Society*, Vol. 49, (1), 2004, pp. 11-27.

[16]Lee, S., “Empirical Wall-Pressure Spectral Modeling for Zero and Adverse Pressure Gradient Flows,” *AIAA Journal*, Vol. 56, (5), 2018, pp. 1818-1829.

[17]Herr, M., Ewert, R., Rautmann, C., Kamruzzaman, M., Bekiropoulos, D., Iob, A., Arina, R., Batten, P., Chakravarthy, S., and Bertagnolio, F., “Broadband Trailing-Edge Noise Predictions - Overview of BANC-III Results,” 21st AIAA/CEAS Aeroacoustics Conference, Dallas, Texas, June 22-26, 2015.

[18]Lee, S., and Shum, J., “Prediction of Airfoil Trailing-Edge Noise Using Empirical Wall-Pressure Spectrum Models,” *AIAA Journal*, Vol. 57, (3), 2019, pp. 888-897.

[19]Hutcheson, F.V., and Brooks, T.F., “Effects of Angle of Attack and Velocity on Trailing Edge Noise,” 42nd AIAA Aerospace Sciences Meeting and Exhibit, Reno, Nevada, January 5-8, 2004.

[20]Chou, S.-T., and George, A.R., “Effect of Angle of Attack on Rotor Trailing-Edge Noise,” *AIAA Journal*, Vol. 22, (12), 1984, pp. 1821-1823.

[21]International Organization for Standardization, “Acoustics - Attenuation of Sound During Propagation Outdoors,” ISO 9613-2, 1996.

[22]Johnson, H.K., and Katz, W.M., “Investigation of the Vortex Noise Produced by a Helicopter Rotor,” USAAMRDL RP 72-2, 1972.

[23]Leverton, J.W., “The Noise Characteristics of a Large ”Clean” Rotor,” *Journal of Sound and Vibration*, Vol. 27, (3), 1973, pp. 357-376.

[24]Drela, M., “XFOIL: An Analysis and Design System for Low Reynolds Number Airfoils,” *Mueller T.J. (eds) Low Reynolds Number Aerodynamics*, Vol. 54, Springer, Berlin, Heidelberg.

[25]Lee, S., “The Effect of Airfoil Shape on Trailing Edge Noise,” *Journal of Theoretical and Computational Acoustics*, 1850020, 2018.